THE AMERICAN SOCIETY OF MECHANICAL ENGINEERS
345 E. 47th St., New York, N.Y. 10017

96-GT-541

THE EFFECT OF PERIODIC RIBS ON THE LOCAL AERODYNAMIC AND HEAT TRANSFER PERFORMANCE OF A STRAIGHT COOLING CHANNEL

G. Rau M. Çakan

D. Moeller T. Arts

von Karman Institute
Belgium

ABSTRACT

The local aerodynamic and heat transfer performance were measured in a rib-roughened square duct as a function of the rib pitch to beight ratio. The blockage ratio of these square obstacles was 10% or 20% depending on whether they were placed on one single (1s) or on two opposite walls (2s). The Reynolds number, based on the channel mean velocity and hydraulic diameter, was fixed at 30000.

The aerodynamic description of the flow field was based on local pressure distributions along the ribbed and adjacent smooth walls as well as on 2D LDV explorations in the channel symmetry plane and in two planes parallel to the ribbed wall(s). Local heat transfer distributions were obtained on the floor, between the ribs, and on the adjacent smooth side wall. Averaged parameters, such as friction factor and averaged heat transfer enhancement factor, were calculated from the local results and compared to correlations given in literature.

This contribution showed that simple correlations derived from the law of the wall similarity and from the Reynolds analogy could not be applied for the present rib height-to-channel hydraulic diameter ratio (e/D_h=0.1). The strong secondary flows resulted in a three-dimensional flow field with high gradients in the local heat transfer distributions on the smooth side walls.

NOMENCLATURE

C_p	pressure coefficient
D_h	hydraulic diameter
e	rib height
f	friction factor
f_0	ref. friction factor in smooth tube (turbulent flow)
Nu	Nusselt number
Nu_0	ref.Nusselt number in smooth tube (turbulent flow)
X,Y, Z	coordinates in streamwise, vertical and lateral directions
U,V,W	streamwise, vertical and lateral velocity components
X_r	separation length, measured from the edge of the rib
X_S	X-position distance from test section entry
Δp	total pressure drop
p_s	wall static pressure
Re	Reynolds number
1s	Ribs on one wall
2s	Ribs symmetric on two opposite walls

INTRODUCTION

The introduction of artificial roughness elements in tubes and rectangular ducts for heat transfer enhancement is found in a wide field of applications, covering e.g. heat exchangers, scram-jet inlets, internal cooling channels of turbine airfoils, etc.

Nikuradse (1950) developed a one-dimensional frictional analysis based on the law of the wall similarity for small sand grain roughness elements in tubes. Dipprey and Sabersky (1963) extended this analysis to a general heat transfer similarity law for roughened tubes similar to the analogy function proposed by Prandtl and Taylor for smooth tubes (see Schlichting, 1982). The effect of the pitch to height variation of ribs in a tube was first studied by Webb et al. (1971); their results were formulated into a correlation. In a next step, Han et al. (1978) performed measurements in a rectangular channel with an aspect ratio of 12.2 and only two ribbed walls. A comparison showed that the aforementioned similarity concept could still be applied for ribs with e/D_h=0.076. Its extension to smaller aspect ratios requested a description of the effect of the presence of the ribbed wall upon the friction and heat transfer characteristics along the smooth wall. This description was proposed by Han (1984) and recently verified by Chandra et al. (1995). The valid range for the application of Han's formula is however limited to $e/D_h \leq 0.0625$.

The larger the rib height and the closer the aspect ratio to unity, the more the flow becomes three-dimensional with accelerations and decelerations in the mainstream direction combined with strong secondary flows. The simple one-dimensional similarity analysis cannot be applied anymore; the complexity of the flow field requires the use of local parameters. Most of the present efforts in numerical flow modeling are limited to two-dimensional approaches on the

Presented at the International Gas Turbine and Aeroengine Congress & Exhibition
Birmingham, UK — June 10-13, 1996
This paper has been accepted for publication in the Transactions of the ASME
Discussion of it will be accepted at ASME Headquarters until September 30, 1996

channel centerline (Liou et al., 1993). Further improvements in the calculation of these flows require information on the local aerodynamic and heat transfer performance. The present experimental program was designed to provide a detailed description of the aerodynamic flow field and to show some links with the local heat transfer performance. A variable heat transfer pattern results in uneven wall temperatures; the latter have to be identified by designers as they may lead to thermal failure of the material. In addition, the applicability of engineering correlations based on the friction similarity law was verified for larger rib heights. Valuable information for code validation was finally provided.

EXPERIMENTAL APPARATUS

High spatial resolution and good optical quality of the channel walls were needed for the aerodynamic investigation whereas limitations in the electrical power supply were imposed for the heat transfer measurements. These requirements finally resulted in the construction of two different large scale test channels.

A. Heat transfer measurements

A sketch of the measurement set-up is shown in Fig. 1. Air at ambient pressure and room temperature was aspirated through a heated test section. This channel, made of plexiglass, had a square cross section (50mm*50mm) and a length of 1000mm. The flow rate was controlled by measuring the wall static pressure downstream of the honeycomb.

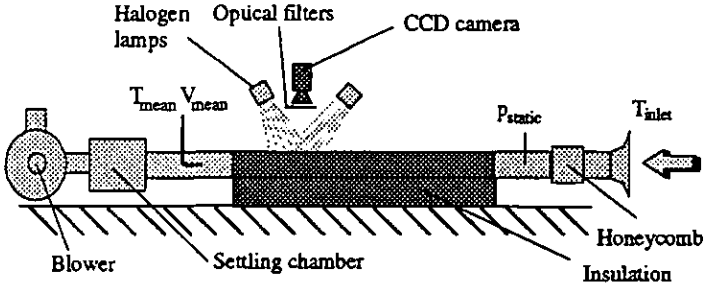

Fig. 1: Heat transfer measurement set-up

A stationary method was used to quantify the wall heat transfer distribution. The wall temperature pattern was provided by liquid crystals. A constant heat flux boundary condition was supplied by the resistive heating of thin inconel sheets, attached to the inner channel walls by an adhesive tape. The ribs, made of plexiglass, had a cross section of 5mm*5mm, were inclined at 90 deg. to the main flow direction and glued with silicone adhesive on the inconel sheets. The composite structure of the walls is summarized in Fig. 2.

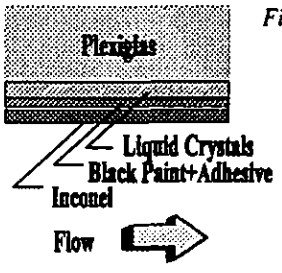

Fig.2: Composite structure of channel walls for heat transfer measurements

The different thickness of the layers were about 50 μm for both the liquid crystal layer and the adhesive tape, and 25 μm for the inconel sheet. Three walls were insulated by foam, the fourth one was not because of optical access.

The color pattern of the liquid crystals was recorded through sharp band optical filters and then transformed, via a calibration curve, into temperatures. This method was initially proposed by Akino (1989).

The conductive heat loss was estimated, from thermocouples buried in the walls, to be around 1.5% of the Joule heating for the insulated walls and around 7% for the non-insulated one. Radiative energy exchanges in the channel were also taken into account. A streamwise linear bulk temperature distribution was assumed and experimentally verified in the test section. The enthalpy rise through the channel was calculated from a heat flux balance and compared to the results given by traversing a combined pressure/temperature probe at the exit of the test section. The detailed determination of the local Nusselt number isolines for ribbed and smooth walls required the adjustment of about four different heating regimes.

B. Aerodynamic measurements

All dimensions of the aerodynamic test section were basically scaled up by a factor of two. The cross section dimensions were 100mm*100mm and the length was 1200 mm. The test section walls were made out of glass. The top wall could be removed and replaced by a plate equipped with tappings for static pressure measurements. The square rib dimensions were 10mm*10mm. The ambient air flow rate was controlled via a static pressure control downstream of the honeycomb.

A TSI 2D-LDV system was used to measure the flow field characteristics. The power output of the argon ion laser was adjusted to 2 Watts for all measurements. The components of the set-up were described by Rau (1995). The optical probe was inclined at 5 deg. to allow a close access to the walls. The length of the probe volume was 1.1mm and its diameter 0.1mm. The seeding consisted of propylene glycol droplets, introduced at the entrance of the wind tunnel. A comparison with the results obtained by a X-hot wire was performed at the beginning of the measurement series. The FFT analysis of the hot wire signal demonstrated that about 800 samples per second were sufficient to capture the high amplitude fluctuations in the flow around a single rib. The average number of samples per channel was adjusted at 6000 to minimize the statistical error on the velocity components and on their RMS value. The comparison of the streamwise normal stress with the X-hot wire results further revealed that no residence time based velocity bias correction should be applied for this kind of flow.

The top wall was replaced by a plate with an array of 66 taps for the pressure measurements. The taps were connected via six scanivalves to two low range (200 Pa) differential pressure transducers. The lateral density of the pressure taps was further increased by allowing a lateral displacement of this instrumented wall. The resulting grid was finally made of 119 measurement points.

C. Measurement stations and data analysis

In order to achieve different p/e ratios the rib height e was kept constant while the pitch p was varied. For a constant channel length this resulted in a different number of ribs in the test section for varying p/e ratios.

The local measurements were performed in a section between two successive ribs. The last rib of the measured section was geometrically fixed at a distance of $10*D_h$. The periodicity of the flow was verified by comparing the flow conditions up- and downstream of this measurement section. The local coordinate system for the measurement section was centered on the symmetry line in the middle of the rib.

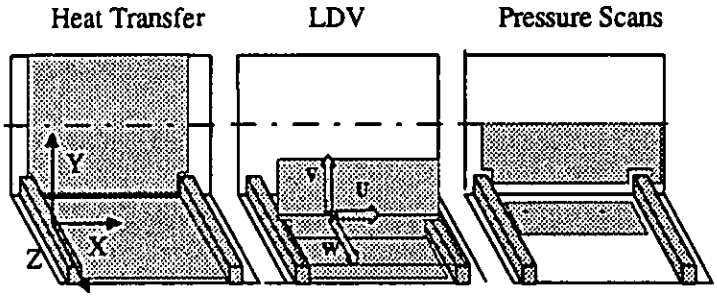

Fig.3: Measurement planes for the three measurement methods

The local Nusselt number distributions were measured on the floor, between the ribs, and on the adjacent smooth side wall for all investigated p/e ratios (Fig. 3). All measured Nusselt number distributions were normalized and presented in terms of enhancement factor with respect to the level obtained in a smooth circular tube (Dittus-Boelter equation).

$$Nu_0 = 0.023 \cdot Re^{0.8} \cdot Pr^{0.4} \qquad (1)$$

Area averaged values were calculated by means of an unstructured grid of triangular cells. The present set-up did not give any information about the heat transfer on the rib itself.

The 2D-LDV measurements were performed in the vertical symmetry plane of the channel and in two planes parallel to the ribbed wall (Fig. 3). Velocity and normal stresses were normalized with the mean bulk velocity calculated from the flow rate.

The static pressure distribution was scanned on the floor between the ribs and on the smooth side wall up to half of the channel height. The friction factor was evaluated from the slope of the static pressure distribution measured over $5*D_h$ along the centerline of the smooth side wall. This approach takes the flow periodicity into account and reduces single reading and rib positioning errors. The definition of the static pressure coefficient and the friction factor are given in eq. (2) and (3).

$$C_p = \frac{p_s - p_{Ref}}{\rho/2 \cdot \overline{U}^2} \qquad (2)$$

$$f = \frac{\Delta p \cdot D_h}{2 \cdot L \cdot \rho \cdot \overline{U}^2} \qquad (3)$$

All presented friction factors are normalized with the friction factor of a smooth tube, given by Blasius

$$f_0 = 0.046 \cdot Re^{-0.2} \qquad (4)$$

The uncertainties in the evaluation of the Nusselt number enhancement ratio and of the friction factor were respectively estimated to be ± 5% and ± 4%, using the analysis proposed by Kline and McClintock (1953). For the velocity measurements, maximum uncertainties of 3% and 4% were respectively estimated for the mean and fluctuation components.

D. Aerodynamic inlet conditions without ribs

Figure 4 presents the measured mainstream mean and fluctuation components at $X_S=2*D_h$ after the test section entry. In this position the flow was turbulent and symmetric, but not fully developed. The boundary layer thickness was about 25% of the hydraulic diameter.

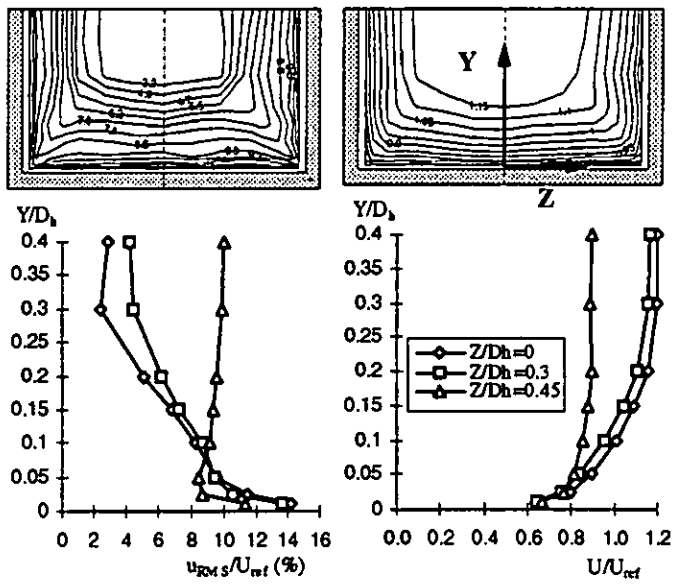

Fig. 4 : Mean and fluctuation comp. of mainstream flow at $X_S=2*D_h$

For the smooth channel it is reasonable to assume that the flow field does not change 2 or $3*D_h$ upstream of this cross section. Velocity measurements in the symmetry plane of the channel showed that periodic flow conditions were achieved after four ribs.

To reproduce these periodic flow conditions we recommend a CFD calculation over five ribs, for which the velocity profiles (Fig. 4) can be used as inlet conditions, $1*D_h$ upstream of the first rib.

ANALYSIS OF THE RESULTS AND DISCUSSION

A. Square channel with ribs on one side

The introduction of ribs locally reduces the cross-section; this results in a main flow acceleration around these obstacles. The sudden expansion downstream of the ribs leads to a separation zone behind them (Fig. 5). After reattachment the entrained flow builds up a new boundary layer. The latter is accelerated by the mainstream through shear forces and impinges on the next rib. The vorticity in this new boundary layer creates a second small vortex in front of the next rib. The flow deflection around the ribs is responsible for high velocity gradients in this zone. The velocity vectors finally indicate the existence of a third small vortex on top of the ribs.

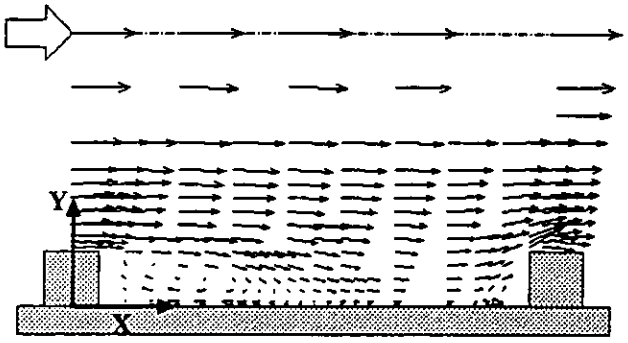

Fig.5: Flow vectors in sym. plane (p/e=9 ; 1s)

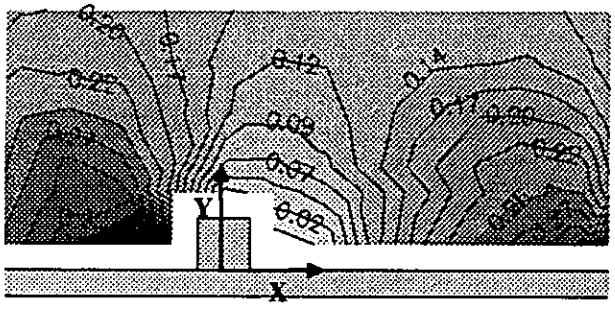

Fig. 6: C_p factor on smooth side wall (p/e=9 ; 1s)

The dominant wall static pressure gradients are observed in the X and Y directions ; the wall static pressure field is basically imposed by the main flow accelerations and decelerations. The static pressure on the floor between the ribs is only slightly increasing in the Z direction towards the smooth side wall. For p/e=12, the measured maximum lateral increase in the static pressure coefficient ΔCp is about 0.04 while the static pressure rise in the X direction along the symmetry line is about ΔCp=0.6. Figure 6 shows the local static pressure coefficient measured on the smooth side wall for p/e=9. The reference pressure is taken at X/e=2, Y/e=0.5. One can essentially distinguish between a high and a low pressure zone respectively in front and behind the ribs. The low pressure zone results from the main flow acceleration and total pressure losses due to the strong gradients in the velocity field around the ribs. The high pressure zone is created by the impingement on the rib and the corresponding main flow deceleration in front of the rib.

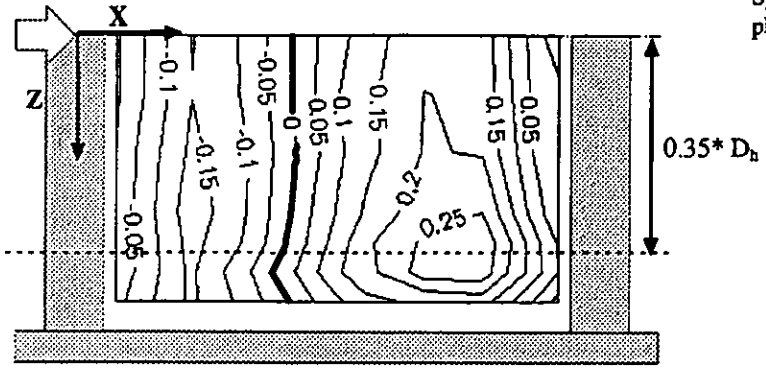

Fig. 7: Normalized U velocity at Y/e=0.25 (p/e=9 ; 1s)

The normalized U velocity isolines in a plane XZ located at Y/e=0.25 are shown in Fig. 7. The maximum values are not along the symmetry line but at Z/D_h=0.35. The lateral displacement of this maximum can be still seen in a XZ plane located at Y/e=1.5. In this plane the maximum U values, again observed at Z/D_h=0.35, are still about 10% higher than those measured on the symmetry line. The extension of the separation bubble in the X direction laterally decreases until Z/D_h=0.4. As a result of the lateral variation it is interesting to state that for the smallest p/e ratio (p/e=6) the flow clearly reattaches around Z/D_h=0.4 while remaining separated in the symmetry plane.

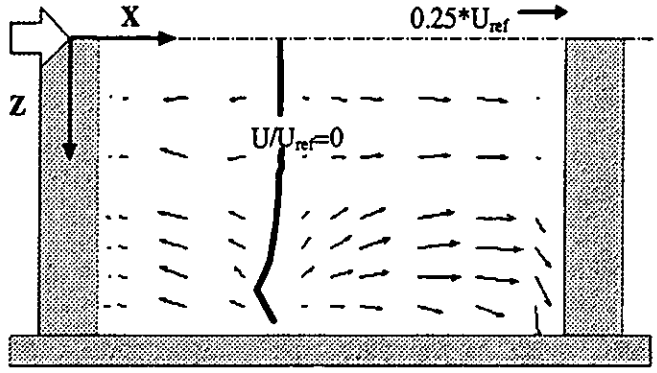

Fig. 8: Velocity vector plot at Y/e=0.25 (p/e=9 ; 1s)

Figure 8 shows the vector representation of the velocity components in the same plane. The entrained main stream flow is displaced by the small lateral pressure gradient towards the symmetry line and turns in front of the next rib towards the side wall.

The secondary flows in YZ cross sectional planes were already measured for rib roughened channels by Hirota et al (1992) and Yokosawa et al (1989). Hirota et al proved the existence of one large vortex cell in each half cross sectional plane of a 1 side ribbed channel. Based on the available information and on our measurements, the three dimensional flow structure observed in a 1 side ribbed channel is sketched in Fig. 9.

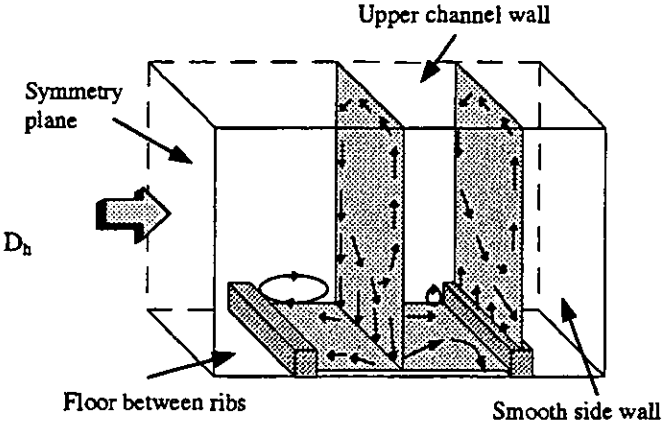

Fig. 9: Sketch of flow field in ribbed channel (1s)

The cross flow moves away from the ribbed floor along the smooth side wall and towards it in the symmetry plane. Liou et al (1993) identified the secondary flow to be turbulence-generated (Prandtl's secondary flows of the second kind). The pressure decrease on the smooth side wall (see Fig. 6) in between the ribs clearly shows that the secondary flow has also a contribution coming from the static pressure field. The downward directed secondary flow motion on top of the rib is deflected towards the smooth side wall by the upward directed wall bounded flow and the low pressure zone on the side wall directly behind the rib. This results in a first strong impingement on the smooth side wall. A second impingement, in front of the rib, was already seen in Fig. 8.

B. Nusselt number enhancement pattern

The ribbed floor Nusselt number enhancement ratio isolines are given in Fig. 10.

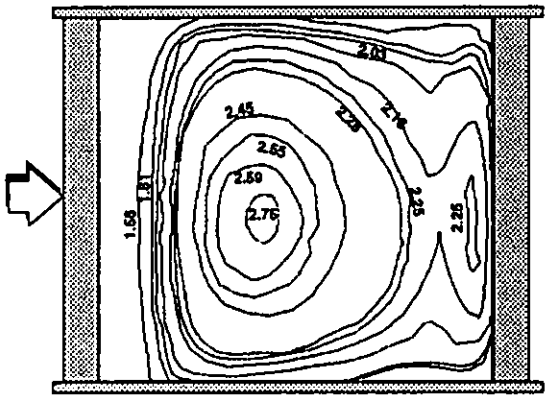

Fig.10: Floor heat transfer enhancement factor isolines (p/e=12)

The zone with maximum heat transfer coincides for all measured configurations with the reattachment zone. The measured normal velocity fluctuations were also maximum in this area. The two dimensional pattern of the Nusselt number enhancement lines (Fig. 10) exhibits important lateral gradients. For higher p/e ratios (p/e≥10) a second maximum is measured in front of the ribs. The distance of this maximum from the rib corresponds to the extension of the separation zone upstream of this obstacle. An almost equivalent isoline pattern is obtained when plotting the turbulence intensity.

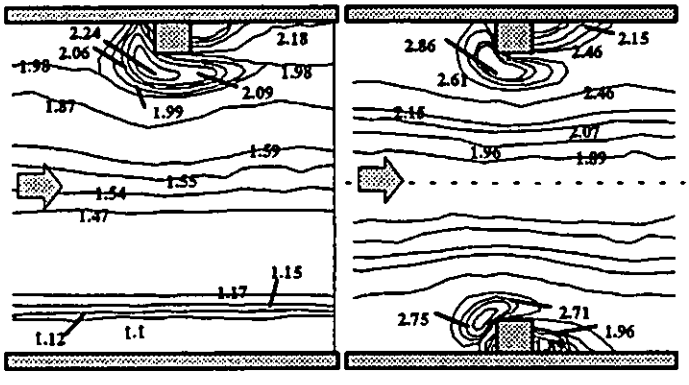

Fig.11a+b: Heat transfer enhancement factor isolines on smooth side wall for one and two opposite ribbed walls (p/e=9)

By looking at the Nusselt number pattern on the smooth side wall (Fig. 11) one can see high heat transfer zones in front and above the ribs. These high heat transfer zones are related to the lateral impingements previously mentioned.

C. Ribs symmetric on two sides

The present pattern does not change considerably for a channel with two opposite walls ribbed. The flow becomes almost symmetric with more pronounced gradients (Fig.11b). Instead of one secondary flow cell per half section one observes one cell per quadrant (see Yokosawa et al., 1989).

D. Local heat transfer performance for 3 different p/e ratios

In the following, the variation of the local heat transfer performance and its link to the local aerodynamic parameters will be discussed for three p/e ratios (6, 9 and 12) in a one side ribbed channel. The heat transfer and static pressure distributinns show the same functional dependencies to p/e for a one and a two side ribbed channel. The two side ribbed channel results will therefore only be presented for p/e=9.

D.1 Local heat transfer on the lateral wall

The local Nusselt number enhancement factor along a vertical line in front of the rib is presented in Fig. 12 for three p/e ratios.

Close to the floor, the ribs at p/e= 9 and 12 provide almost an equivalent enhancement, slightly superior to the case of p/e=6. The location of the maximum in the Y direction is the same for all investigated p/e values (Y/D_h=0.1). This maximum can be explained by the previously mentioned deflection of fluid towards the smooth side wall (see also Fig. 13). This lateral impingement becomes smaller with increasing Y/D_h ratio>0.15.

Above Y/D_h=0.4 the heat transfer performance is independent from p/e. In this region the heat transfer is mainly influenced by turbulent momentum exchange. Note that the measured turbulence intensities on the channel centerline (Y/D_h=0.5) do not change either for the three p/e ratios (Fig. 14).

The rib placement on two opposite walls leads to higher peak velocities and higher turbulence intensities so that the overall heat transfer performance is increased (Fig. 12).

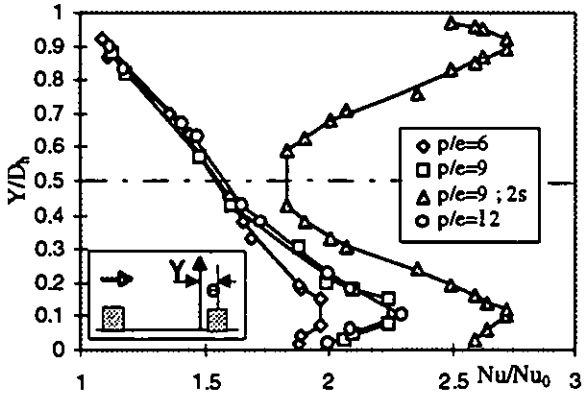

Fig.12: Heat transfer enhancement along a vertical line on the smooth side wall

The lateral W velocity was measured along a line above the rib (Y/e=1.5) and close to the smooth side wall (Z/D_h=0.45) (Fig. 13). The magnitude of the lateral velocities is about the same for p/e=9 and 12 and smaller for p/e=6. The maximum value on top of the rib is about 17% of the mean bulk velocity. In a parallel plane at Y/e=0.5 the maximum W/U_{ref} ratio increases to about 0.22 in front of the rib (see Fig. 8).

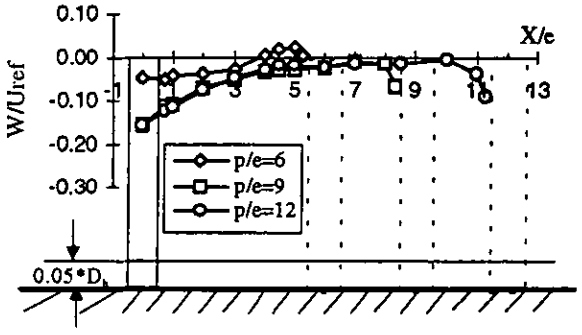

Fig.13: Lateral normalized velocity component at Y/e=1.5 ; Z/D_h=0.45

Besides the impingement on the smooth side wall, the high turbulence intensities have a favorable effect on the heat transfer (Maciejewski et al., 1992). The measured RMS values on the centerline (Y/D_h=0.5, Z/D_h=0) of the channel are given in Fig. 14. All curves present a minimum in between the ribs but no remarkable difference in the turbulence intensity was seen for the investigated p/e ratios. The normalized fluctuation components in X and Y directions were about 12.5% and 8.5%. The well known anisotropy in the normal stresses was observed in all measurement planes.

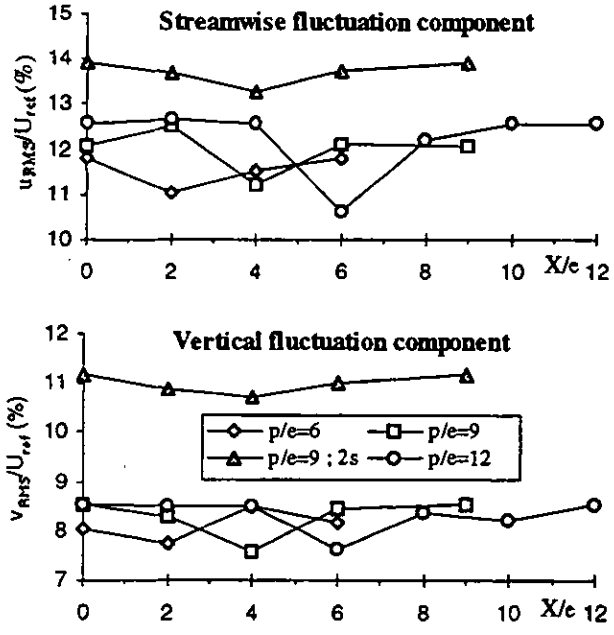

Fig.14: Measured fluctuation components in the channel center (Y/D_h=0.5 ; Z/D_h=0)

D.2 Local heat transfer along the symmetry line of the ribbed floor

The Nusselt number enhancement factor along the symmetry line on the ribbed floor is shown in Fig. 15. The maximum value of its distribution as well as of its increase after the rib were smallest for p/e=6. The p/e ratios of 9 and 12 provided about the same enhancement factor gradient but the maximum was higher for p/e=12.

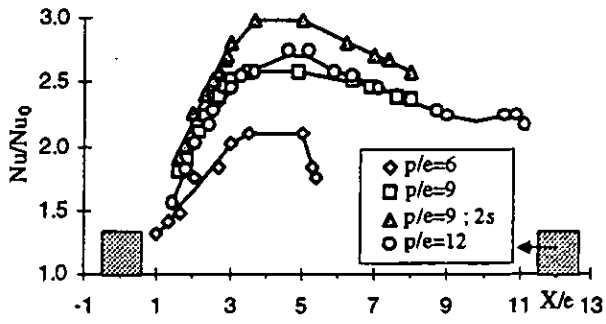

Fig. 15: Heat transfer increase along the centerline of the floor

The location of the maximum heat transfer zone corresponded to the position of the reattachment point. The length of the separation zone downstream of the rib was measured with the LDV system at a distance of Y/e=0.05 in the symmetry plane; it was defined by the interval in which the U velocity remained negative. The distance of this interval from the edge of the rib became larger for increasing p/e ratios: $3.75<X_r/e<4.0$ for p/e=8, $4.0<X_r/e<4.25$ for p/e=9,10,12 and $4.25<X_r/e<4.5$ for p/e=14,16. The same trend was also found by Okamoto et al. (1994). For a two side ribbed channel with p/e=9 the reattachment distance was reduced by $\Delta X_r/e$=0.25. The extension of the second separation zone in front of the rib was found to be 1-1.5 times the rib height for p/e=8, 9 ,10, 12 and in between 0.5-1 times the rib height for p/e=14, 16.

In between the two separation zones a new boundary layer was built up by the entrained flow. In order to overcome the pressure rise in streamwise direction the main flow above the ribs has to energize the flow in the new boundary layer through the shear layer behind the rib crest. The acceleration of this boundary layer flow is shown in Fig. 16 at a vertical distance of Y/e=0.1 .

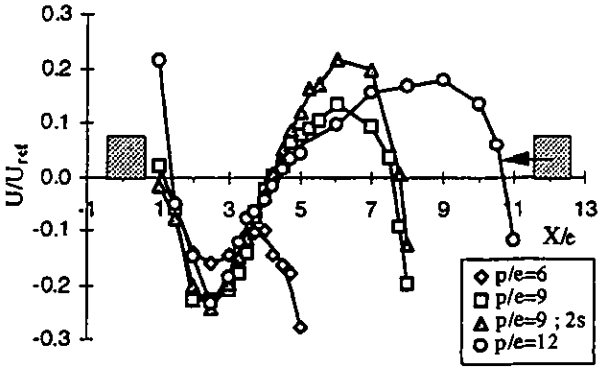

Fig. 16: U component at Y/e=0.1 in the symmetry plane

In the case of a one side ribbed channel, the velocity gradient immediately after the reattachment was strongest for p/e=9. Considering that the adverse pressure gradient was almost the same for all investigated p/e ratios lead to the conclusion that the momentum transfer through the shear layer was also maximum for this p/e ratio. A longer distance between the reattachment point and the next rib leads to a higher maximum velocity for larger p/e ratios. The vertical V velocity on this line (Y/e=0.1) was slightly negative at X/e=4.75 and its absolute value remained in a band of ±1% (or ±2%) of the mean channel velocity for the one (or two) side ribbed channel up to distance from the next rib of ΔX=1.5e.

Vogel et al. (1985) showed in their experiment behind a backward facing step that the effective origin of the redeveloping thermal boundary layer lies approximately two step heights downstream of reattachment. Assuming a similar behavior for the ribbed case and considering the limited extension of the new developing boundary layer creates strong doubts about the applicability of the Reynolds analogy to the floor heat transfer for the investigated p/e ratios.

The vertical motion in the separation behind the rib, the secondary flows as well as the increased cross section lead to a displacement of cold mainstream towards the ribbed wall. This relative cold fluid reduces the local bulk temperature and consequently increases the driving temperature difference. This is shown in Fig. 17, preseating the vertical velocity component at the rib crest (Y/e=1). The maximum vertical velocity was slightly higher for p/e=9 compared to 6 and 12.

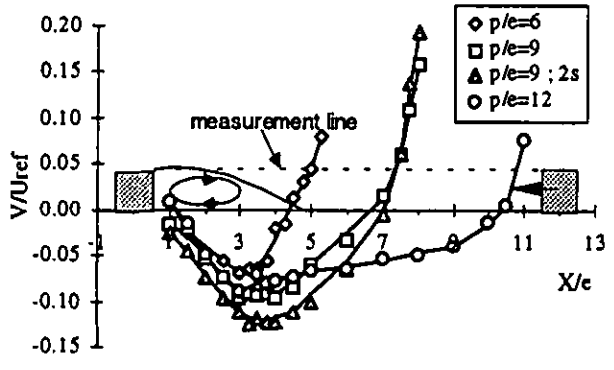

Fig.17: Flow entrainment in between the ribs at Y/e=1 in sym. plane

The RMS-values of the vertical velocity component at a distance of Y/e=0.3 are presented in Fig. 18 as another parameter for heat transfer enhancement. The same maximum value of Tuy=16.5% was measured at the edge of the recirculation zones for all three p/e ratios. A shorter recirculation zone was observed for a two side ribbed channel ($\Delta X_r \approx 0.25*e$). The rate of decay of these fluctuations was independent of p/e and after attaining a minimum they were again amplified by the second separation zone in front of the ribs.

In vertical direction the fluctuations were maximum in the shear layer behind the rib. For the one side ribbed channel the maximum values for p/e=6, 9, 12 were Tux_{max}=26%, 28%, 28% and Tuy_{max}=16%, 18%, 18%. For the 2 sides ribbed channel with p/e=9 they increased to Tux_{max}=35% and Tuy_{max}=24%.

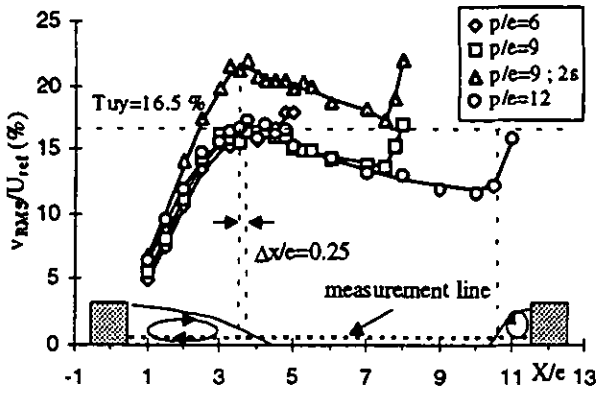

Fig.18: Vertical fluctuation component in between the ribs at Y/e=0.3 in sym. plane

D.3 Friction factor analysis

While in a smooth channel the measured pressure drop can directly be linked to the shear stress at the wall, this is not true for a ribbed channel. The impingement in front of the rib leads to a local high static pressure in this zone, while the flow acceleration on top of the rib, in combination with high local total pressure losses, resulting from strong velocity gradients, gives a local low pressure zone behind the rib (Fig. 19). The resulting force is defined in the literature as form drag (Lewis, 1975).

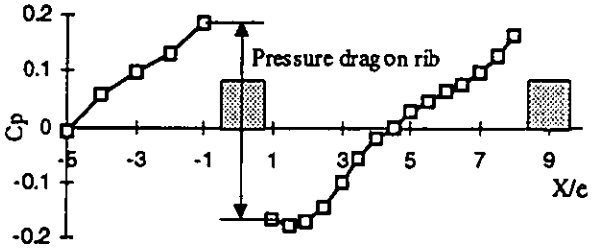

Fig. 19: Floor pressure distribution on the symmetry line (p/e=9 ; 1s)

The friction factor, calculated from the measured total pressure drop, is therefore the sum of the averaged skin friction and this rib form drag. For the application of the Reynolds analogy, it is interesting to quantify the contribution of this rib form drag on the measured total pressure drop. The rib form drag can be also easily used for numerical code validation because it contains all irreversible effects which have to be modeled correctly around the rib.

In order to simplify the measurement set-up a new definition of this rib form drag is proposed. This simplified rib form drag is calculated from the pressure difference between two taps on the floor centerline at a distance 0.5*e before and after the rib. If the streamwise static pressure changes between these taps and the rib are negligible and if the pressure on the rib side walls is constant, this definition is equivalent to the physical rib form drag.

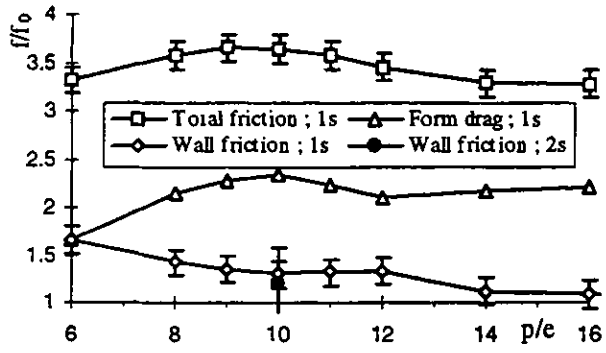

Fig.20: Friction factor variation for one side ribbed channel

Fig. 20 compares, for the one side ribbed channel, the friction factor calculated from the total pressure drop with the rib form drag. Both present a peak around p/e=9. The rib form drag is the dominant contribution to the total friction factor for almost all investigated configurations.

Subtracting the form drag from the total friction factor gives the averaged skin friction factor. The results indicate that the averaged skin friction is decreasing with increasing p/e. The averaged skin friction enhancement for p/e=9 is found to be about 1.3, compared to a smooth channel. The same calculation for a two side ribbed channel with symmetric and staggered rib arrangements gives values of respectively 1.05 and 1.2. Considering the total magnitude of the measured total friction factor enhancement of 9.5±0.4 (Fig. 21), this result shows the large contribution of the rib form drag to the measured friction factor.

Furuya et al. (1976) found the same result for a flat plate roughened by two-dimensional wires. They measured the static pressure distribution on the wire itself. The subtraction of the form drag coefficient from the flow resistance coefficient gave a frictional contribution which did not differ from that of a smooth plate. The variation of the flow resistance and pressure drag coefficient with p/e was similar to the reported results in Fig. 20 with a maximum for p/e=8.

D.4 Comparison of global performance parameters to results in literature and correlations

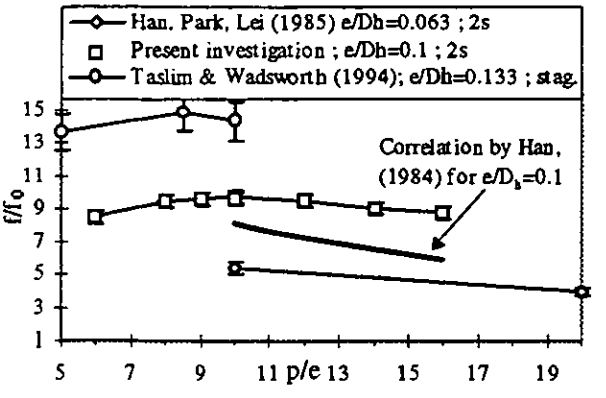

Fig.21: Friction factor enhancement for a two side ribbed channel

The total friction factor for a two side ribbed channel is given in Fig. 21. The comparison to the literature shows a good fit of the present data with results from previous investigations for different e/D_h ratios. The correlation, given by Han et al. (1984), underestimates for the present e/D_h ratio of 0.1 the total pressure loss in the channel. The measured local heat transfer distributions were averaged on the floor and the smooth side wall for all investigated p/e ratios (Fig. 22).

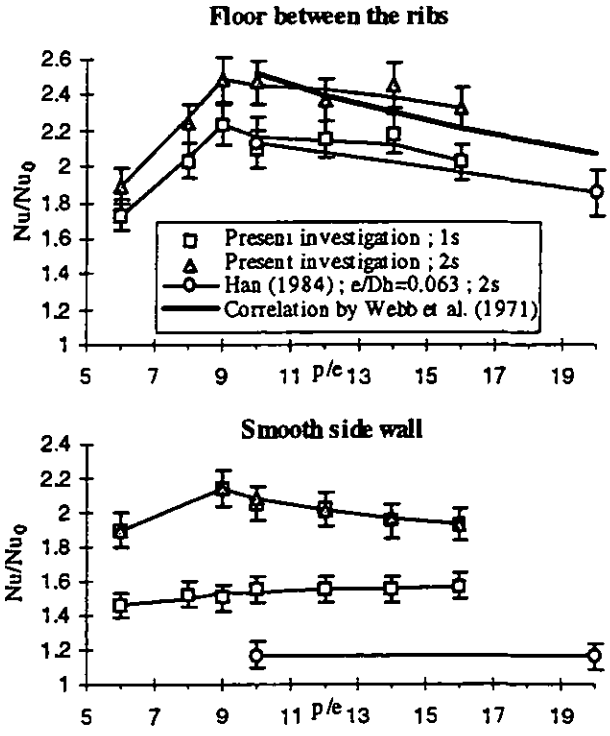

Fig. 22: Average heat transfer enhancement

The ratio between the averaged heat transfer enhancement on the smooth side wall and on the ribbed wall was about 70% for the one side ribbed channel and about 85% for a channel with two opposite ribbed walls. The comparison to previous investigations shows that the decrease in heat transfer performance with increasing p/e ratio was about the same for all, although the e/D_h ratio was different. It can be further seen that the increase in e/D_h ratin was more favorable for the heat transfer performance on the smooth side wall than on the ribbed wall.

The correlation of Webb et al. (1971), estimating the overall heat transfer enhancement of a ribbed tube, is also included in Fig. 22a. His exponential fit correlated quite well with the averaged floor data of the two side ribbed channel. The approximation by Han (1984), that the overall heat transfer enhancement can be described by an area weighted average between the results of Webb's correlation and the heat transfer of a smooth tube is not appropriate for higher e/D_h ratios. The application of this correlation must be limited to the validated range of $0.021 \le e/D_h \le 0.063$ given by Han (1984).

CONCLUSIONS

Detailed aerodynamic and heat transfer measurements were performed in a square channel with ribs presenting a significant

blockage ratio (e/D_h=0.1). The results of the local measurements were discussed for three different p/e ratios (6, 9, 12) in a one side ribbed channel. The differences with a two side ribbed channel were given for p/e=9.

The description of the flow characteristics showed that the flow structure is three-dimensional around the rib with significant lateral velocity components and a displacement of the maximum streamwise velocity towards the smooth side wall.

The pressure field in between the ribs amplified the Reynolds stress induced secondary flows, while the low pressure zone on top of the rib deflected the secondary flow towards the smooth side wall. A second impingement on the smooth side wall was observed in front of the rib.

Both impingements favored the heat transfer on the smooth side wall in front and on top of the rib and a proportionality between the lateral velocity and the heat transfer enhancement was found.

The local heat transfer enhancement distribution on the symmetry line showed a slightly better performance for p/e=12. The averaging over all floor data gave on the contrary a maximum for p/e=9. This example indicated the difficulty of deriving general conclusions from partial information.

The maximum acceleration of new boundary layer flow for p/e=9 in close proximity to the wall behind the reattachment indicated that the shear forces in the shear layer behind the rib was maximum for this p/e ratio.

Neither the turbulence intensities in the channel center nor on the symmetry line in proximity of the floor between the ribs differed significantly for varying p/e ratios.

A new definition of the rib form drag simplified the required measurement set-up ; its physical significance favored it for numerical code validation. The large contribution of this rib form drag to the total pressure loss emphasized the importance of the rib shape for larger e/D_h ratios and denied a direct link between the measured friction factor and the heat transfer performance via the Reynolds analogy.

The comparison of Webb's correlation and Han's approximation to the averaged measurement data showed, that its range of validity could not be extended to rib height to hydraulic diameter ratios of 0.1.

The present understanding of this very complex flow field and the limitation of the existing correlations stresses the importance of further developments in numerical analysis to develop tools which are not limited to global performance estimations but capture local effects and allow to compute more realistic configurations. The presented measurement data is a contribution to the validation of these CFD-codes.

ACKNOWLEDGMENT

The authors express their gratitude to SNECMA and TURBOMECA for the partial financial support in the present investigation.

REFERENCES

AKINO, N.; ICHIMIYA, K.; MITSUSHIRO, K.; UEDA, M. (1989) ; Improved Liquid-Crystal Thermometry excluding Human Color Sensation ; J.Heat Transfer, Vol. 111 , No.2, pp. 558-565

CHANDRA, P.R.; NILAND, M.E.; HAN, J.C. (1995) ; Turbulent Flow Heat Transfer and Friction in a rectangular Channel with varying Number of ribbed Walls ; ASME Paper No. 95-GT-13

DIPPREY, D.F.; SABERSKY,R.H (1963) ; Heat and Momentum Transfer in Smooth and Rough Tubes at various Prandtl Numbers ; Int. J. Heat Mass Transfer, Vol. 6, pp. 329-353

FURUYA,Y.; MIYATA, M.; FUJITA, H. (1976) ; Turbulent Boundary Layer and Flow Resistance on Plates Roughened by Wires ; J.Fluids Engineering, pp.635-644

HAN, J.C.; GLICKSMAN, L.R.; ROHSENOW, W.M. (1978) ; An Investigation of Heat Transfer and Friction for Rib-Roughened Surfaces ; J.Heat Mass Transfer, Vol. 121, pp. 1143-1156

HAN, J.C (1984) ; Heat Transfer and Friction on Channels with two opposite Rib-Roughened Walls ;J.Heat Transfer,Vol. 106, pp.774-781

HAN, J.C.; PARK, J.S.; LEI, C.K. (1985) ; Heat Transfer Enhancement in Channels with Turbulence Promoters ; J. of Engineering for Gas Turbines and Power, Vol. 107, pp.628-635

HIROTA, M.; YOKOSAWA, H. ; FUJITA, H.M. (1992) ; Turbulence Kinetic Energy in turbulent flows through Square Ducts with rib-roughened Walls ;Int. J.Heat and Fluid Flow,Vol. 13, No.1 , pp. 22-29

KLINE, S.J.; McCLINTOCK, F.A. (1953) ; Describing Uncertainty in Single-Sample Experiments ; Mechanical Engineering, Vol. 75, Jan. 1953, pp. 3-8

LEWIS, M.J. (1975) ; An Elementary Analysis for Predicting the Momentum- and Heat-Transfer Characteristics of a Hydraulically Rough Surface ; J. Heat Transfer, pp.249-254

LIOU, T.-M.; WU, Y.-Y.; CHANG, Y. (1993) : LDV-measurements of periodic fully developed Main and Secondary Flows in a Channel with Rib-Disturbed Walls ; ASME J.of Fluids Engeering, Vol 115, pp.109-114

MACIEJEWSKI,P.K.; MOFFAT, R.J. (1992) ; Heat Transfer with very high Free-Stream Turbulence: Part II ; J. Heat Transfer, Vol.114, pp. 834-839

NIKURADSE, J. (1950) ; Laws for Flow in rough Pipes ; NACA TM 1292

OKAMOTO, S.; TSUNODA, K.; KATSUMATA, T.; SUZUKI, D. ; ABE, N; (1994) ; Turbulent Shear Flow over the repeated two-dimensional square Ribs on Ground Plane ; Presented at 7th inter. Symp. on appl. of Laser Techniques to Fluid Dynamics, Lisbon

RAU (1995) ; The Blockage Effect of Turbulators in a Rectilinear Cooling Channel ; Presented at VKI Lecture Series 1995-05 ; Brussels

SCHLICHTING, H (1982) ; Grenzschicht-Theorie ; G.Braun Karlsruhe

TASLIM, M.E.; WADSWORTH, C.M.; (1994) ; An experimental Investigation of the Rib Surface-Averaged Heat Transfer Coefficient in a rib-roughened Square Passage ; ASME Paper No. 94-GT-162

VOGEL, J.C.; EATON, J.K. (1985) ; Combined Heat Transfer and Fluid Dynamic Measurements Downstream of a Backward-Facing Step ; J.Heat Transfer, Vol. 107, pp. 922-929

WEBB, R.L.; ECKERT, E.R.G.; GOLDSTEIN, R.J. (1971) ; Heat Transfer and Friction in Tubes with Repeated-Rib Roughness ; Int. J. Heat Mass Transfer, Vol. 14, pp. 601-617

YOKOSAWA, H.; FUJITA, H.; HIROTA, M.; IWATA, S.; (1989) ; Measurements of Turbulent Flow in a Square Duct with roughened Walls on two opposite Sides ; Int. J. Heat and Fluid Flow, Vol. 10, No.2, pp. 125-130